Analysis and Prediction of Instability Waves within High-Speed Flow Over Sharp and Blunt Cones with Plasma Actuation

Jianhui Cheng and Steven A. E. Miller

University of Florida
Department of Mechanical and Aerospace Engineering
Theoretical Fluid Dynamics and Turbulence Group

Florida Fluids Symposium
May 2022

Acknowledgements

The authors are grateful for continuous funding from Space Research Initiative (SRI) OR-DRPD-SRI2020: Reduction of Rocket Vibrations via Control of Large-Scale Coherent Turbulent Structures.

Outline

- Introduction and Background
- Methodology
  - Instability Wave Theory
  - Pressure Fluctuations from Instability Waves
  - Phenomenological Plasma Actuator Model
- Results and Analysis
  - Stability Properties
  - Spatial Coherence of Base Flow
  - Effects of Plasma Actuation
  - Spatial Coherence of Actuated Flow
- Summary and Conclusion

Background

Fig 1. Launch of Orbital ATK's Antares rocket[1].

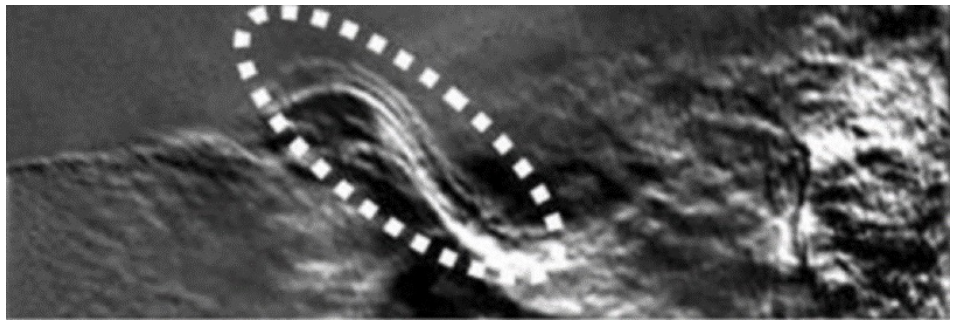

Fig 2. A schlieren of jet moving left to right where a large instability wave is circled. Courtesy of Prof. Mitchell.

- Aerodynamic loading on the flight-vehicle surface causes intensive vibration and cabin noise
- Instability waves that lead to transition to turbulence create large pressure fluctuations on the surface of vehicles
- Nose bluntness affect the stability and transition
- Objective: to further study the effects of nose bluntness within high-speed boundary layer flows via computing the pressure fluctuations from the instability waves on cones with different nose radii and plasma actuation

[1] Lubert, C. P., "Sixty Years of Launch Vehicle Acoustics," Acoustic Society of America, Vol. 31, 2017.

Instability Wave Theory

- Governing Equations[2]

$$\frac{\partial \rho}{\partial t} + \nabla \cdot (\rho u) = 0$$

$$\rho\left[\frac{\partial u}{\partial t} + (u \cdot \nabla)u\right] = -\nabla p + \nabla \cdot [\lambda(\nabla \cdot u)I] + \nabla \cdot [\mu(\nabla u + \nabla u^{tr})]$$

$$\rho c_p\left[\frac{\partial T}{\partial t} + (u \cdot \nabla)T\right] = -\nabla \cdot (k\nabla T) + \frac{\partial p}{\partial t} + (u \cdot \nabla)p + \Phi$$

- Procedure
  - Linearize: $u = \bar{u} + \tilde{u}, T = \bar{T} + \tilde{T}$,etc.
  - Parallel flow: $\bar{u} = \bar{u}(y), \bar{T} = \bar{T}(y)$, etc.
  - Nondimensional: edge value, $l = \sqrt{v_e^* x^* / u_e^*}$
  - Sutherland's law: $\bar{\mu} = \bar{T}^{3/2} \frac{1 + C/T_\infty^*}{\bar{T} + C/T_\infty^*}$
  - $\tilde{k} = \frac{d\bar{k}}{d\bar{T}} \tilde{T}$

- Instability Wave Formulation

$$\widetilde{\phi}(x, y, z, t) = \widehat{\phi}(y) \exp(i(\alpha x + \beta z - \omega t))$$

  - α, β are the wavenumber
  - $\widehat{\phi}(y)$ is shape function

- Linear Stability Equations System

$$\left(A\frac{d^2}{dy^2} + B\frac{d}{dy} + C\right)\hat{\phi} = 0$$

  - Boundary conditions

$$y = 0,\ \hat{\phi}_1 = \hat{\phi}_2 = \hat{\phi}_3 = \hat{\phi}_5 = 0$$

$$y \to \infty, \hat{\phi}_1, \hat{\phi}_2, \hat{\phi}_3, \hat{\phi}_5 \to 0$$

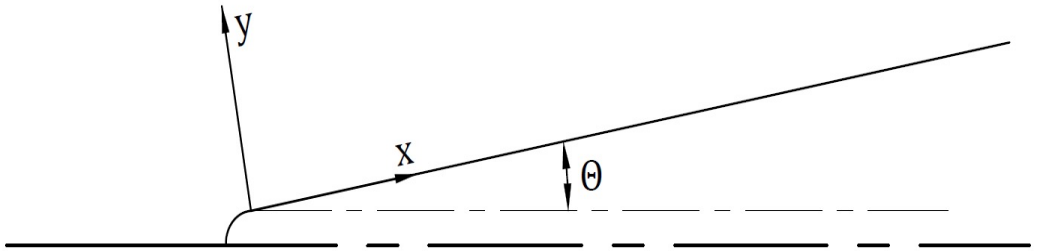

Fig 3. Coordinate system.

Pressure Fluctuations from Instability Waves

- Wall Pressure Fluctuations Construction[3]

$$\tilde{p}(x,y,z,t) = \int_{-\infty}^{\infty} \hat{p}(y)\exp[i(\alpha x + \beta z - \omega t)]d\omega$$

Maximum growth rate at azimuthal direction is chosen.

- Spatial Coherence

$$\Gamma(\boldsymbol{\xi},\omega) = \frac{1}{2\pi}\int_{-\infty}^{\infty} \langle \tilde{p}(\boldsymbol{x},t), \tilde{p}(\boldsymbol{x}+\boldsymbol{\xi}, t+\tau)\rangle \exp(-i\omega\tau)\, d\tau$$

- Cross-Power Spectral Density (CPSD)

$$\Psi_{pp}(\boldsymbol{\xi},\omega) = \phi(\omega)\Gamma(\boldsymbol{\xi},\omega)$$

- Phenomenological Plasma Actuator Model[4]

$$S_v = \frac{Q}{\pi^{3/2}a^3}\exp\left(-\frac{d^2}{a^2}\right), d = \sqrt{(x-x_c)^2 + (y-y_c)^2 + (z-z_c)^2}$$

[2] Malik, M. R., and Spall, R. E., "On the Stability of Compressible Flow Past Axisymmetric Bodies," Journal of Fluid Mechanics Digital Archive, Vol. 228, 1991, pp. 443–463.
[3] Zhou, H., "Coherent Structure Modeling and its Role in the Computation of Passive Quantity Transport in Turbulent Flows." JSME International Journal Series B, Vol. 41, No. 1, 1998, pp. 137–144.
[4] Poggie, J., "Plasma-Based Hypersonic Flow Control," 37th AIAA Plasmadynamics and Lasers Conference, AIAA Paper No. 2006-3567, 2006.

Flow Conditions

- Flow Conditions[5] and nose radii

M_∞	T_∞(K)	ρ_∞(kg/m3)	Re(1/m)	L(m)	r_n(mm)
3.5	90.1	0.0874	9.45×10^6	0.3556	0.038

r_1	r_2	r_3	r_4	r_5	r_6	r_7	r_8	r_9	r_{10}
0.038	0.076	0.152	0.38	1.14	1.905	3.969	7.938	15.876	38.1

- Cone Configuration and Grid Distribution

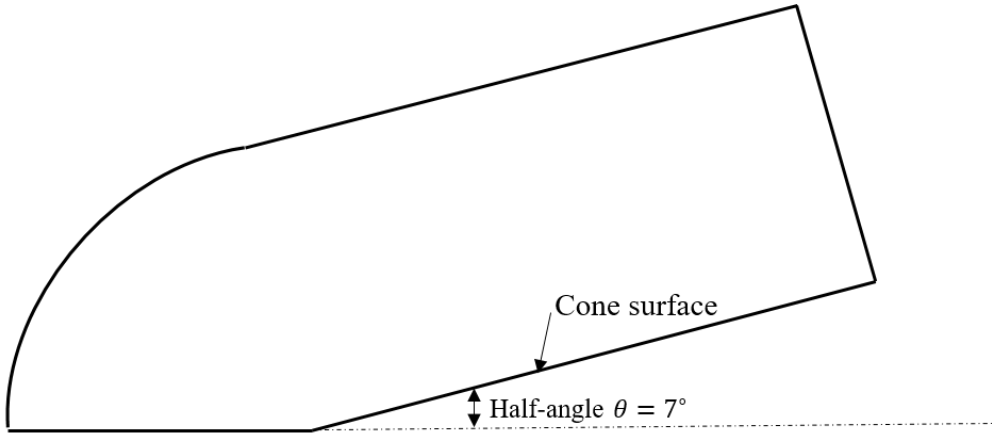

Fig 4. Flow region.

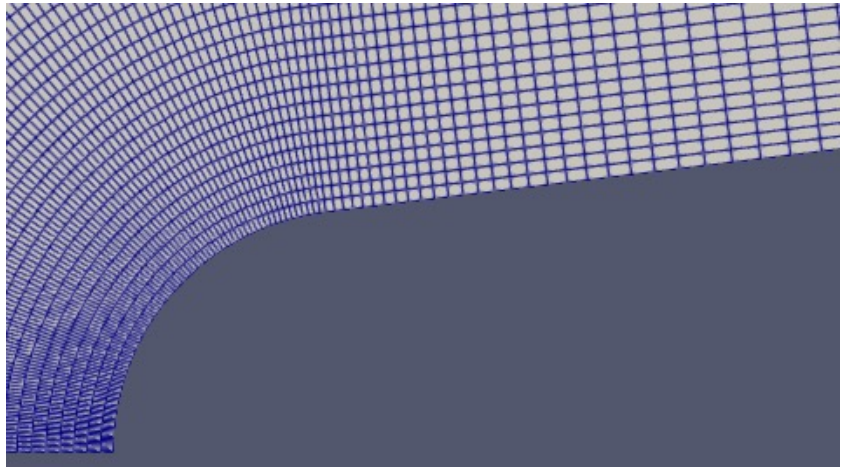

Fig 5. Nose region.

[5]Gross, A., and Fasel, H. F., "Numerical Investigation of Supersonic Flow for Axisymmetric Cones," Mathematics and Computer sin Simulation, Vol. 81, No. 1, 2010, pp. 133–142.

Stability Properties

- Maximum Growth Rate Distribution

  Mack-mode: $0 < f^* < 75\text{kHz}$, $0 < n < 40$

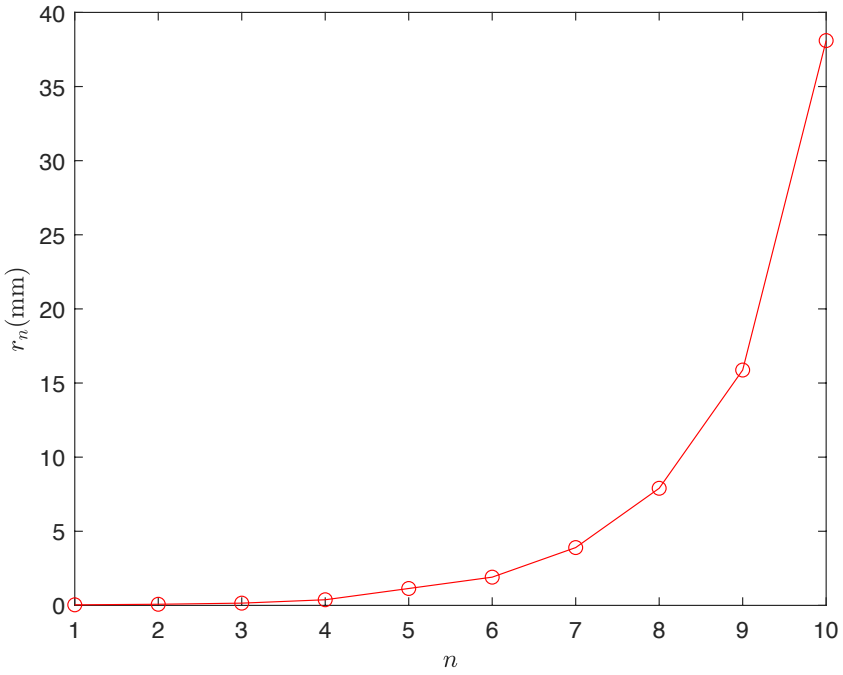

Fig 9. Nose radii distribution.

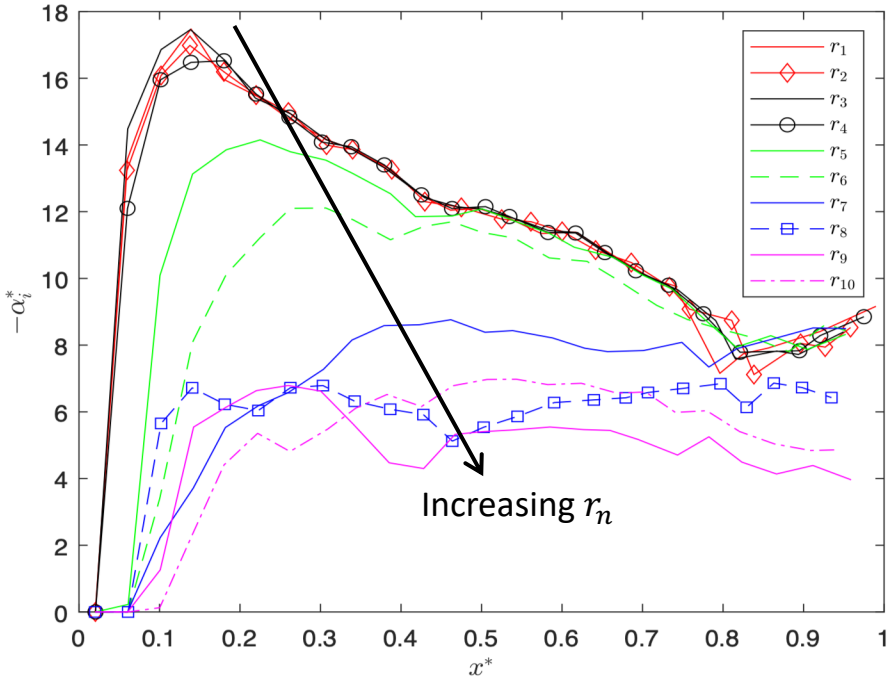

Fig 10. Maximum growth rates over all frequencies (f^*) and azimuthal mode number (n).

- Small nose radii do not alter the maximum growth rate and peak locations close to the leading edge ($r_1 \sim r_4$) ;
- Large nose radii have small growth rate due to thick boundary layer and peak locations moves downstream ($r_4 \sim r_7$);
- Complex growth rates distribution in larger nose radii ($r_7 \sim r_{10}$).

Spatial Coherence of Base Flow

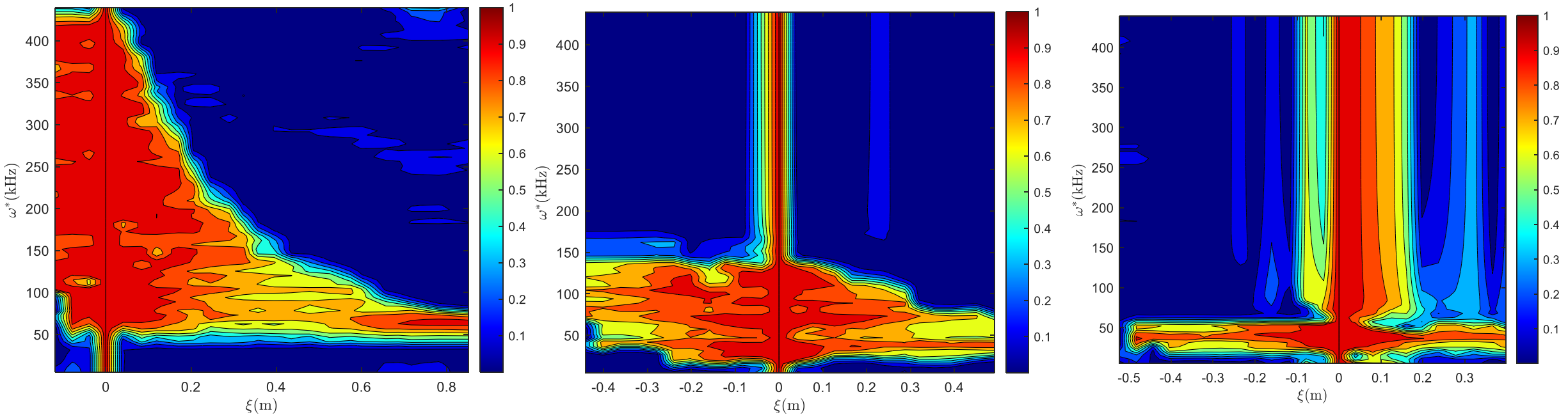

$r_1 = 0.038$ mm $\quad r_7 = 3.969$ mm $\quad r_{10} = 38.1$ mm

Fig 11. Spatial coherence of r_1, r_7, and r_{10} at $M_\infty = 3.5$, where the reference point of each case is the position of maximum growth rate in the streamwise direction.

- Amplified instability waves have higher spatial coherence
- Growth rates depend on the non-dimensional frequency $\omega = \frac{2\pi f^* l}{u_e^*}$ and $l = \sqrt{\nu_e^* x^* / u_e^*}$

J. Cheng and S. A. E. Miller, University of Florida, Department of Mechanical and Aerospace Engineering, chengjianhui@ufl.edu

Effects of Plasma Actuation

$Q = 100$ W, $y_c = 0.008$ m, $a = 0.005$ m, x_c is the position of maximum growth rate of each case

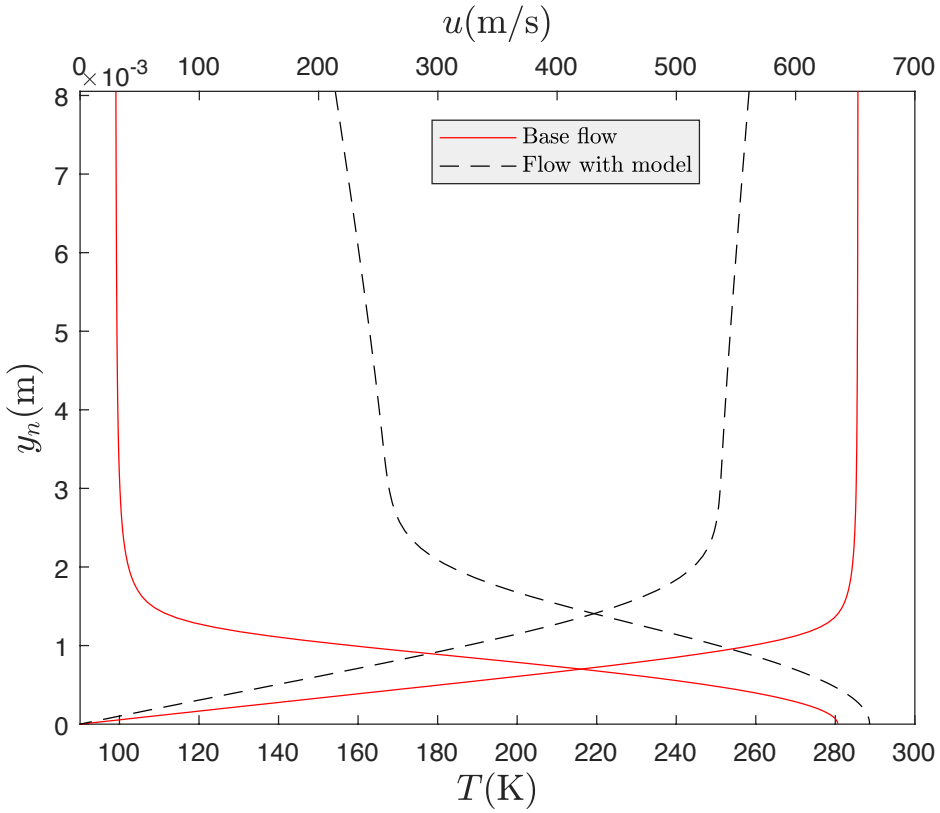

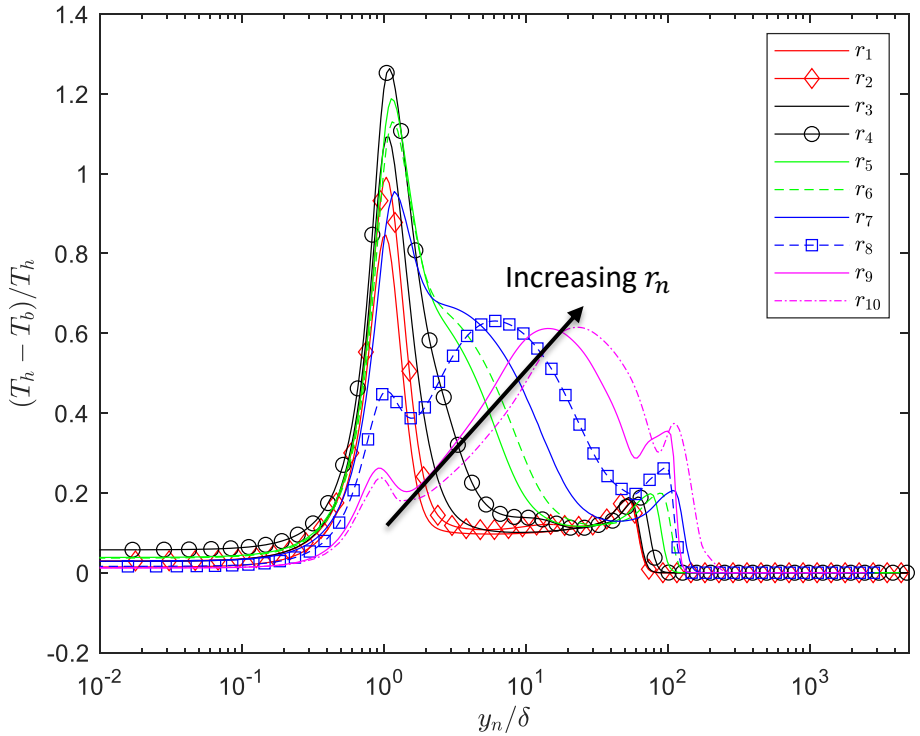

Fig 12. Mean flow field comparison between base flow and flow with actuation (Left) and relative temperature difference between base flow and flow with actuation (Right)

- Temperature increase and velocity decrease
- Relative temperature difference increase for blunt cone due to entropy layer

J. Cheng, University of Florida, Department of Mechanical and Aerospace Engineering, chengjianhui@ufl.edu

Effects of Plasma Actuation

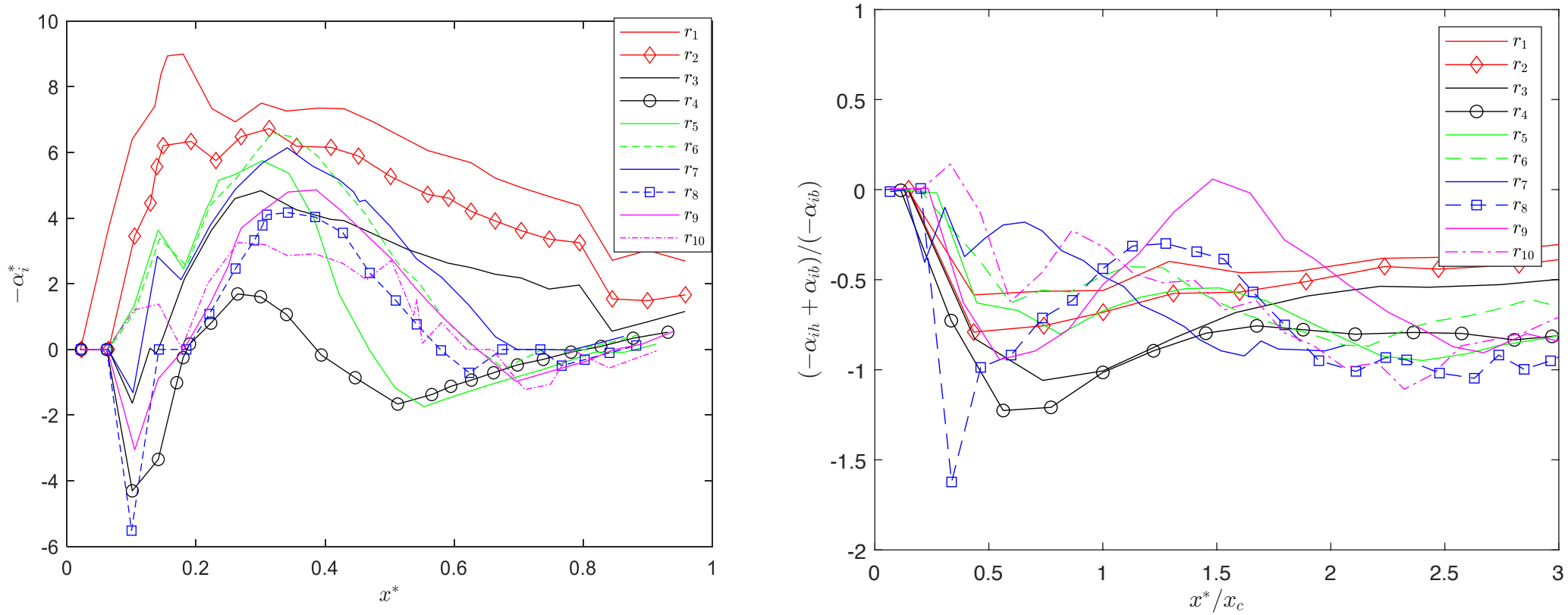

Fig 13. Growth rates distribution along streamwise direction of flow with plasma actuation (Left) and relative growth rates between base flow and flow with actuation (Right)

- Plasma actuation stabilize the flow-field
- Growth rates decrease with same plasma actuator with increasing nose radii ($r_1 \sim r_4$)

Spatial Coherence of Actuated Flow

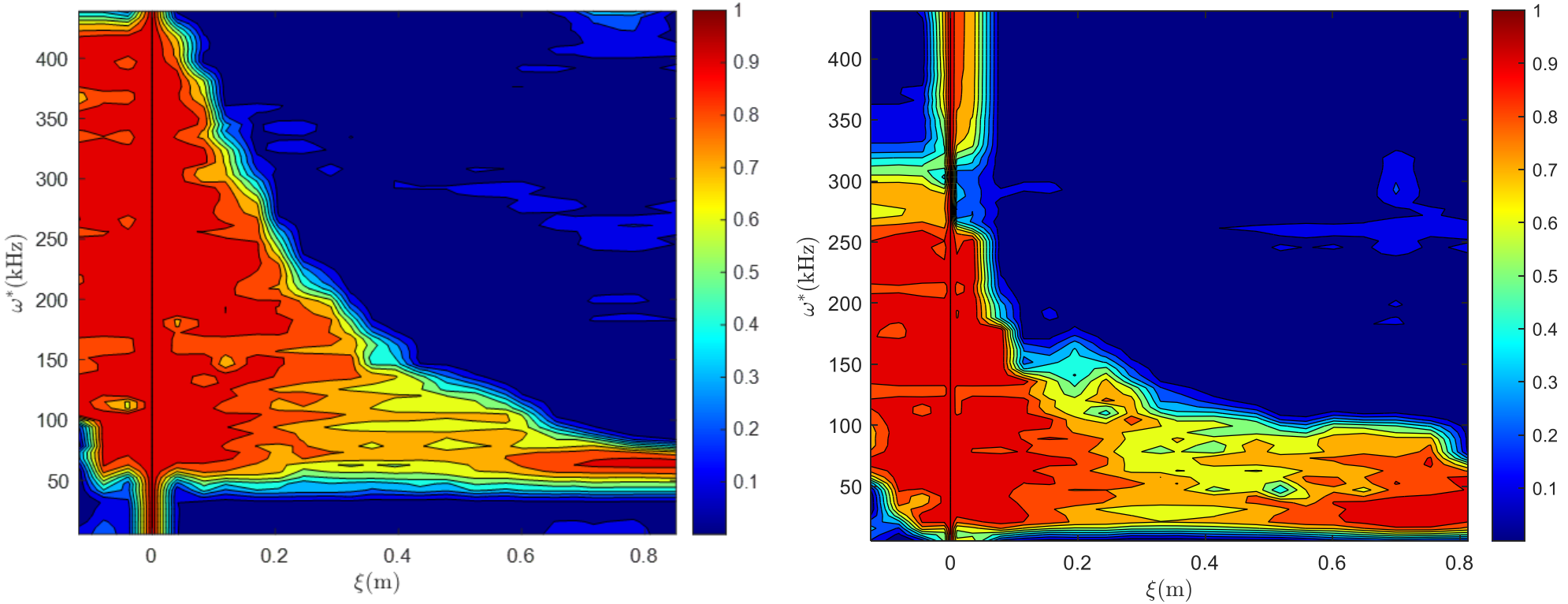

Fig 14. Spatial coherence of base flow (left) and actuated flow (right) for $r_1 = 0.038$ mm, where the reference point of each case is the position of maximum growth rate in the streamwise direction.

- Growth rates depend on the non-dimensional frequency $\omega = \frac{2\pi f^* l}{u_e^*}$ and $l = \sqrt{\nu_e^* x^* / u_e^*}$, u_e^* decrease
- Compared with base flow, the frequency range become smaller and move to low frequency

J. Cheng, University of Florida, Department of Mechanical and Aerospace Engineering, chengjianhui@ufl.edu

Summary and Conclusion

- Summary and Conclusion
  - Linear stability solver is applied to compute the growth rate distribution
  - The small nose radii would not affect the maximum growth rate and spatial coherence
  - The large nose radii have higher spatial coherence within a smaller frequency range
  - The plasma actuation adds heating, stabilizes the flow-field, and decreases the frequency range of spatial coherence
- Future Work
  - Study the effects of positions of plasma actuator model on flow-fields and stability properties

Thank you!

Questions?